# FLUID ANTENNA SYSTEMS UNDER $\alpha$-$\mu$ FADING: PERFORMANCE ANALYSIS AND LIQUID NEURAL NETWORKS-BASED PORT SELECTION FOR MULTIPLE ACCESS

PEDRO DUARTE ALVIM

MASTER'S THESIS
IN ELECTRICAL ENGINEERING

DEPARTMENT OF ELECTRICAL ENGINEERING

FACULTY OF TECHNOLOGY

UNIVERSITY OF BRASÍLIA

University of Brasília
Faculty of Technology
Department of Electrical Engineering

# Fluid Antenna Systems under $\alpha$-$\mu$ Fading: Performance Analysis and Liquid Neural Networks-Based Port Selection for Multiple Access

Pedro Duarte Alvim

MASTER'S THESIS SUBMITTED TO THE POST-GRADUATE PROGRAM IN ELECTRICAL ENGINEERING OF THE UNIVERSITY OF BRASÍLIA AS PART OF THE REQUIREMENTS NECESSARY TO OBTAIN THE MASTER'S DEGREE.

APPROVED BY:

---

Hugerles Sales Silva, Dr. (University of Brasília)
(Supervisor)

---

Ugo Silva Dias, Dr. (University of Brasília)
(Co-supervisor)

---

Edson Porto da Silva, Dr. (Federal University of Campina Grande)
(External Examiner)

---

André Antônio dos Anjos, Dr. (Federal University of Uberlândia)
(External Examiner)

Brasília/DF, March/2025.

**FICHA CATALOGRÁFICA**

ALVIM, PEDRO

Fluid Antenna Systems under $\alpha$-$\mu$ Fading: Performance Analysis and Liquid Neural Networks-Based Port Selection for Multiple Access . [Brasília/DF] 2025.

viii, 51p., 210 x 297 mm (ENE/FT/UnB, Master, Master's Thesis, 2025).

University of Brasilia, Faculty of Technology, Department of Electrical Engineering.

Department of Electrical Engineering

1. $\alpha$-$\mu$ Distribution
2. Fluid Antenna Systems
3. Telecommunications
4. Performance Metrics
5. Port Selection
6. Machine Learning

I. ENE/FT/UnB

II. Título (série)

**REFERÊNCIA BIBLIOGRÁFICA:**

ALVIM, PEDRO (2025). Fluid Antenna Systems under $\alpha$-$\mu$ Fading: Performance Analysis and Liquid Neural Networks-Based Port Selection for Multiple Access . Master's Thesis, Department of Electrical Engineering, Publication PPGEE DM-827/25, University of Brasília, Brasília, DF, 44p.



---

Pedro Alvim

Universidade de Brasília (UnB)

Campus Darcy Ribeiro

Faculdade de Tecnologia - FT

Departamento de Engenharia Elétrica (ENE)

Brasília - DF, CEP 70919-970

# RESUMO

**Sistemas De Antenas Fluidas Sob Desvanecimento $\alpha$-$\mu$: Análise De Desempenho E Seleção De Portas Baseadas Em Redes Neurais Líquidas Para Acesso Múltiplo**

Neste estudo, estatísticas de primeira e segunda ordem são deduzidas para sistemas de antenas fluidas (FAS) sob canais sujeitos ao desvanecimento $\alpha$-$\mu$. Com base nisso e para avaliar o desempenho dos mencionados sistemas, expressões também são deduzidas para a probabilidade de indisponibilidade (OP) e a capacidade ergódica do canal. Além disso, uma redução exata da OP devido à $N$-ésima porta para uma $(N-1)$-porta também é apresentada. Este trabalho também enquadra o problema de seleção de porta como uma tarefa de classificação multirrótulo pela primeira vez, melhorando a seleção da melhor porta com um número de observações de porta limitadas. Este desafio é abordado alavancando redes neurais líquidas (LNNs) para prever a porta ideal sob cenários emergentes de acesso múltiplo de antena fluida (FAMA) juntamente com um modelo de desvanecimento $\alpha$-$\mu$ mais generalista. Uma otimização de hiperparâmetros para refinar as arquiteturas LNN sob diferentes cenários de observação é aplicada. Várias curvas, corroboradas por simulações de Monte-Carlo, são mostradas sob diferentes valores para os parâmetros do sistema e do canal. Todas as expressões emergentes deste trabalho são novas, marcando uma contribuição significativa para o corpo de conhecimento existente. Este é o primeiro trabalho em que o efeito da não linearidade do canal é evidenciado em FAS ou FAMA.

Palavras-chave: Capacidade ergódica do canal, FAMA, FAS, LNN, OP, seleção de porta.

# ABSTRACT

In this study, first and second order statistics are deduced for fluid antennas systems (FAS) under $\alpha$-$\mu$ fading channels. Based on this and in order to evaluate the performance of the mentioned systems, expressions are also deduced for the outage probability (OP) and ergodic channel capacity. Furthermore, an exact reduction of the OP due to $N$-th port for an $(N-1)$-port is also presented. This work also frames the port selection problem as a multi-label classification task for the first time, improving best-port selection with limited port observations. This challenge is addressed by leveraging liquid neural networks (LNNs) to predict the optimal port under emerging fluid antenna multiple access (FAMA) scenarios alongside a more general $\alpha$-$\mu$ fading model. Hyperparameter optimization to refine LNN architectures for different observation scenarios is applied. Several curves, corroborated by Monte-Carlo simulations, are shown under different values for the system and channel parameters. All the expressions emerging from this work are entirely new, marking a significant contribution to the existing body of knowledge. This is the first work in which the effect of the channel non-linearity is evidenced in a FAS or FAMA.

Keywords: Ergodic channel capacity, FAMA, FAS, LNN, OP, port selection.

# CONTENTS

# LIST OF FIGURES

# LIST OF SYMBOLS

| | |
|---|---|
| $\alpha$ | Non-linearity of the channel |
| $\mu$ | Number of multipath clusters |
| $N$ | Number of ports |
| $W$ | Constant linear dimension |
| $\lambda$ | Wavelength |
| $k$ | Specific port |
| $\delta_k$ | Power correlation coefficient for each port |
| $\delta$ | Power correlation coefficient for all ports |
| $J_0(\cdot)$ | Zero-order Bessel function of the first kind |
| $J_1(\cdot)$ | First-order Bessel function of the first kind |
| ${}_a\mathrm{F}_b(\cdot;\cdot;\cdot)$ | Generalized hypergeometric function |
| $y_k$ | Received signal at the $k$-th port |
| $x$ | Transmitted signal |
| $g_k$ | Complex envelope fading at the $k$-th port |
| $h_k$ | Normalized envelope fading at the $k$-th port |
| $\eta_k$ | Complex additive white Gaussian noise at the $k$-th port |
| $e$ | Euler's number |
| $\exp(\cdot)$ | Exponential function |
| $f_{h_k}(\rho_k)$ | Probability density function |
| $F_{h_k}(\rho_k)$ | Cumulative distribution function |
| $\Gamma(\cdot)$ | Gamma function |
| $\Gamma(\cdot,\cdot)$ | Upper incomplete Gamma function |
| $\gamma(\cdot,\cdot)$ | Lower incomplete Gamma function |
| $\mathrm{I}_v(\cdot)$ | Modified Bessel function of first kind and order $v$ |
| $\mathrm{Q}_\mu(\cdot,\cdot)$ | Marcum Q-function |
| $\rho_{\mathrm{th}}$ | Threshold level |
| $L(\rho_{\mathrm{th}})$ | Level crossing rate |
| $\dot{(\cdot)}$ | Derivative form |
| $\gamma$ | Instantaneous SNR or SINR |
| $\gamma_{\mathrm{th}}$ | SNR or SINR OP threshold |
| $\bar{\gamma}$ | Average signal-to-noise ratio |
| $P_{\mathrm{out}}$ | Outage probability |
| $\Delta P_{\mathrm{out}}$ | Exact reduction of outage probability |
| $C$ | Ergodic capacity |
| $U$ | Number of users |
| $s_u$ | Symbol transmitted to the $u$-th user |
| $\mathbb{E}(\cdot)$ | Expectance operator |

| | |
|---|---|
| $(\cdot)^*$ | Complex conjugate |
| $(\cdot)^\dagger$ | Transpose |
| $M$ | Number of best ports |
| $\arg\max(\cdot)$ | Argument that the maximum operator finds |

# GLOSSARY

| | |
|---|---|
| 5G | Fifth-generation |
| 5G+ | Fifth-generation and beyond |
| 6G | Sixth-generation |
| AFD | Average fade duration |
| AWGN | Additive white Gaussian noise |
| BS | Base station |
| CDF | Cumulative distribution function |
| cGAN | Conditional generative adversarial network |
| CNN | Convolutional neural network |
| CSI | Channel state information |
| DNN | Dense neural network |
| FAMA | Fluid Antenna Multiple Access |
| FAS | Fluid Antenna System |
| LCR | Level crossing rate |
| LNN | Liquid Neural Network |
| LSTM | Long short-term memory |
| LTC | Liquid time constant |
| MIMO | Multiple-input multiple-output |
| ML | Machine Learning |
| MLC | Multi-label classification |
| MRC | Maximum ratio combining |
| MSE | Mean square error |
| NOMA | Non-orthogonal multiple access |
| ODE | Ordinary differential equation |
| OP | Outage probability |
| PCA | Principal component analysis |
| PDF | Probability density function |
| RIS | Reconfigurable intelligent surfaces |
| s-FAMA | Slow fluid Antenna Multiple Access |
| SINR | Signal-to-interference-plus-noise ratio |
| SNR | Signal-to-noise ratio |
| SPO | Smart, predict, and optimize |
| THz | Terahertz |
| UAV | Unmanned aerial vehicle |

CHAPTER 1

# INTRODUCTION

## 1.1 SCOPE AND RELATED WORKS

Fluid antenna system (FAS) is an emerging topic and has been studied by several researchers over the past years [1, 2, 3, 4, 5, 6, 7, 8, 9, 10, 11, 12, 13, 14, 15], with potential application in the new emerging wireless technologies and being, recently, proposed as a possible solution to overcome the physical limitation of space present in multiple-input multiple-output (MIMO) systems [3]. The existing literature presents various works on fluid antennas, shedding light on their capabilities and potential applications for fifth generation (5G) and beyond (5G+/6G).

In [1], the concept of FAS is discussed. Wong *et. al.* [1] devised a system in which a single antenna can change its position instantly in a linear space and named it FAS. In the aforementioned work, the receiving antenna is isotropic and its location can be switched between one of the $N$ possible predefined locations, also called ports. In turn, the performance limits of the mentioned systems are introduced in [2], in which expressions are presented for the level crossing rate (LCR), the average fade duration (AFD) and ergodic channel capacity for the $N$-port FAS. In addition, a closed-form capacity lower bound is also presented in [2]. Expressions for the probability density function (PDF) and cumulative distribution function (CDF) of the envelopes at all the ports for the FAS are deduced in [3], considering correlated Rayleigh fading channels. An exact, approximated and upper bound expressions are derived for the outage probability (OP).

FAS are studied in [4] over correlated Nakagami-$m$ fading channels. New expressions for the PDF and CDF are derived by the authors and the performance of the mentioned system is also assessed by OP. Closed-form expressions are deduced in [5] in order to characterize the LCR, considering the practical constraints and limitations. In [2, 3, 4, 5], it should be noted that the same correlation model between the ports is considered, which has the disadvantage of

requiring a reference port. In order to solve this problem, a more realistic model for correlation is presented in [16], in which there is no need for a reference port (*i.e.*, any port is a reference to another port). FAS has been studied in different contexts and scenarios, such as multiple access [6, 7], large-scale cellular networks [9], maximum ratio combining (MRC) [17] and MIMO evolution beyond 5G through reconfigurable intelligent surfaces (RIS) [10].

Recently, FAS has been adapted for multi-user access, known as fluid antenna multiple access (FAMA) [6, 7, 8], which exploits different user-fading envelopes to enable efficient multi-user connections with low processing demands. FAMA provides very high data speed and low latency, as well as supports high link density, high energy and spectral efficiency, high reliability, and high mobility [18]. This is important to achieve the 5G+/6G requirements and enables FAMA to be combined with technologies such as deep learning, artificial intelligence, MIMO, NOMA, RIS, and terahertz communication. This combination makes it possible for FAMA to be applied to real-world solutions such as smart grid, internet of things, industrial internet, smart city, smart transportation, and smart health. Several challenges and solutions for real scenarios in which FAMA can be applied are described in [18]. In FAS and FAMA, it is assumed that the system can select the port with the best signal-to-noise ratio (SNR) and signal-to-interference-plus-noise ratio (SINR), respectively [6, 7, 8]. However, with a large number of ports $N$, obtaining channel state information (CSI) for all ports in real-time within the coherence time is impractical. Therefore, a critical challenge in FAS is the port selection problem, in which the system must determine the optimal antenna's port to maximize signal quality. This problem is even more challenging in FAMA, which must maximize signal quality and minimize interference across multiple simultaneously served users with distinct fading profiles. Due to the difficulty of obtaining signal quality or CSI for all ports, advanced techniques, such as machine learning (ML), are essential to efficiently select the best port based on limited observations (*i.e.*, observing only a small percentage of ports). Solving this problem is key to maximizing FAS and FAMA performance in next-generation networks.

In the literature, the port selection problem in FAS and FAMA has been investigated in several studies [11, 12, 19, 20, 21]. In [11], ML methods such as long short-term memory (LSTM) and a novel algorithm called smart, predict, and optimize (SPO) are used to predict the optimal port in FAS by observing only a fraction of ports. The results in [11] show a reduction in OP,

even with only 10% of the ports being observed. In [11], the correlation model adopted by the authors has the disadvantage of requiring a reference port, which is a simplistic and unrealistic assumption. In [12], the port selection problem in FAS is revisited, also considering the use of LSTM and SPO algorithms, but adopting a more realistic correlation model [16], where any port can be a reference for another one. LSTM is applied under a slow FAMA scenario in [19], considering a more accurate model to emulate spatial correlation across the ports. The aforementioned work obtained good results with only 25% of the ports observed. In [20], an LSTM-based learning approach is considered to estimate and predict the CSI of the port for fast selection in FAS, exploring the temporal and spatial correlation of the channels. In [21], the SINR is inferred from only a few observations in fluid antennas using conditional generative adversarial network (cGAN), where OP improvements are obtained. The port selection problem is framed as a regression task in all these related works. Moreover, they all adopt correlated Rayleigh fading.

## 1.2 OBJECTIVES

This work has two main objectives. The first one is to provide analytical and simulation results to reveal how the channel non-linearity affects FAS performance. The second objective is to treat the port selection problem as a multi-label classification (MLC) task, improving best-port selection with limited port observations. This challenge is addressed by leveraging LNNs to predict the optimal port under emerging FAMA scenarios alongside a more general fading model.

## 1.3 ORIGINAL CONTRIBUTIONS

This manuscript is based on the work presented in papers published in top journals in the field of this thesis. The main contributions of this studies are:

- Chapter 2 presents: (i) new expressions for the first order statistics, such as PDF and CDF; and for the second order statistics, such as LCR; of the envelopes at all the ports; (ii) new expressions for OP and ergodic channel capacity; (iii) an exact reduction of

the OP due to $N$-th port for an $(N-1)$-port; (iv) an evaluation of the impact of the correlation coefficient between the ports on the performance of FAS.

- Chapter 3 analyzes: (i) the port selection problem as a MLC task for the first time, improving best-port selection with limited port observations; (ii) the use of LNNs to predict the optimal port; under FAMA scenarios, including MRC; and a more general $\alpha$-$\mu$ fading model; (iii) the use of hyperparameter optimization to refine LNN architectures for different observation scenarios; (iv) the impact of $\alpha$-$\mu$ fading in port selection.

## 1.4 PUBLICATIONS

1. P. D. Alvim *et al.* Sistemas de Antenas Fluidas sob Desvanecimento Weibull e Diferentes Modelos de Correlação. *XLI Simpósio Brasileiro de Telecomunicações e Processamento de Sinais*, Out. 2023.

2. P. D. Alvim *et al.* On the Performance of Fluid Antenna Systems under $\alpha$-$\mu$ Fading Channels. *IEEE Wireless Communications Letters*, vol. 13, no. 1, pp. 108-112, Jan. 2024.

3. P. D. Alvim *et al.* LNN-powered Fluid Antenna Multiple Access. *IEEE Wireless Communications Letters*, Under review, pp. 1-5, Jan. 2025.

## 1.5 DOCUMENT ORGANIZATION

This document is organized into four chapters, described as follows: Chapter 1 starts by recalling the scope and state-of-the-art concerning works that deal with FAS. Finally, the objective and structure of this document is presented.

Chapter 2 presents a study about FAS under $\alpha$-$\mu$ fading channels, in which new expressions for relevant first and second order statistics are derived. Furthermore, system metrics expressions are also deduced to evaluate the performance. Several curves are shown under different values for the system and channel parameters.

Chapter 3 expands the port selection problem as a MLC task, marking a novel approach to

improving best-port selection with limited port observations. To address this issue, LNNs are used to identify the optimal port in dynamic FAMA environments, incorporating the generalist $\alpha$-$\mu$ fading model. Furthermore, LNN architectures are optimized through hyperparameter tuning.

Chapter 4 presents the conclusions derived from the results and the recognition of their significance within this dissertation regarding FAS and FAMA from multiple perspectives. Additionally, it outlines potential future research directions to contribute to the advancement of the scientific community.

CHAPTER 2

# ON THE PERFORMANCE OF FLUID ANTENNA SYSTEMS UNDER $\alpha$-$\mu$ FADING CHANNELS

**Motivation and Outline**

Concerning the literature review, it is observed that all available works on FAS consider simple fading models, such as Rayleigh or Nakagami-$m$. However, the mentioned models characterize only the multipath effect. Over the years, several studies have explained that wireless communication channels can also be affected by the non-linearity of the propagation medium. Thus, not incorporating the effect of non-linearity in the models is not a realistic assumption.

In this context, the performance of FAS under $\alpha$-$\mu$ fading channels is evaluated in this work. Several new expressions for the first and second order statistics are deduced and used to derive OP and ergodic channel capacity metrics for evaluate the mentioned systems. In this study, the $\alpha$-$\mu$ distribution is adopted to characterize the small-scale fading. The $\alpha$-$\mu$ channel model [22] has been extensively supported by experimental results in the technical literature, including terahertz (THz) [23]. Furthermore, it is written in terms of physical parameters and adopted in many works. In addition, the $\alpha$-$\mu$ jointly considers the multipath fading and the non-linearity of the propagation medium, that makes this distribution able to model realistic environments [22]. As the $\alpha$-$\mu$ encompass other models as special cases, it should be mentioned that this study is connected with other works, such as [2, 3, 4], in which some results can be obtained as a particular case of the study presented in this work.

To the best of author knowledge, all the expressions emerging from this study are entirely new, marking a significant contribution to the existing body of knowledge. Several curves are shown under different values for the system parameters and channel non-linearity. This is the first work in which the effect of the channel non-linearity is evidenced in a FAS and thus, this work open new fronts for further investigations

## 2.1 SYSTEM AND CHANNEL MODELS

### 2.1.1 Fluid Antennas Systems

A FAS is considered in this work, based on [3]. In the mentioned system, there are $N$ different fixed locations for the best reception of the signal, distributed over a linear dimension $W\lambda$, in which $\lambda$ is the wavelength and $W > 0$ is a constant related to the size of the FAS, as see in Fig. 2.1. It should be mentioned that each location is referred as port and an antenna at location port $k$ is considered as an ideal point antenna.

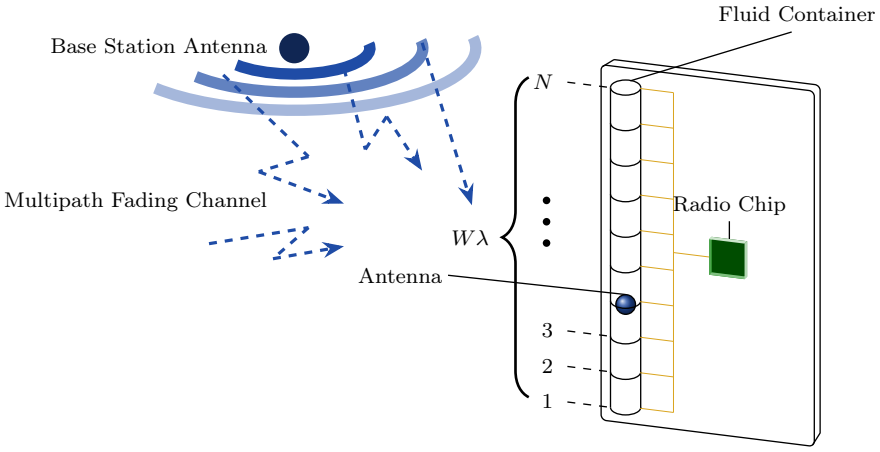


**Figure 2.1.** A possible architecture for a FAS.

### 2.1.2 Correlation Models

In this work, the mathematical models for the correlation between the ports ($\delta_k$) presented in [2] and [16] are considered. In [2], the first port is the reference location and the other $N-1$ ports are correlated to the first one. In a FAS, the correlation effect occurs since the ports are close to each other. The power correlation coefficient, denoted by $\delta_k$, is written as

$$\delta_k = J_0^2\left(\frac{2\pi(k-1)W}{N-1}\right), \; k = 2, \ldots, N. \tag{2.1}$$

In (2.1), $J_0(\cdot)$ is the zero-order Bessel function of the first kind.

In this study, a realistic power correlation coefficient model is also considered. In [16], a common correlation coefficient ($\delta = \delta_k$) between all ports is adopted, in which there is no need for a reference port (i.e., any port is a reference to another port). The power correlation

coefficient $\delta$ is written as [16, Eq. (5)]

$$\delta = 2\left[{}_1\mathrm{F}_2\left(\frac{1}{2};1;\frac{3}{2};-\pi^2W^2\right) - \frac{J_1(2\pi W)}{2\pi W}\right], \forall\, k, \tag{2.2}$$

where $J_1(\cdot)$ is the first-order Bessel function of the first kind [27, id 03.01.02.0001.01] and ${}_{\mathrm{a}}F_{\mathrm{b}}(\cdot;\cdot;\cdot)$ represents the generalized hypergeometric function.

### 2.1.3 Received Signal and Fading Models

The received signal at the $k$-th port in a FAS is given by [3, Eq. (3)]

$$y_k = g_k x + \eta_k, \tag{2.3}$$

in which $x$ is the transmitted signal, $\eta_k$ is the zero-mean $\sigma_\eta^2$-variance complex additive white Gaussian noise (AWGN) at the $k$-th port, and $g_k$ is the complex envelope fading, where $h_k \triangleq |g_k|/\sqrt[\alpha_k]{\mathrm{E}[|g_k|^{\alpha_k}]}$ is the normalized envelope, modeled in this study by the $\alpha$-$\mu$ distribution, whose PDF is given by [22, Eq. (3)]

$$f_{h_k}(\rho_k) = \frac{\alpha_k \mu^\mu \rho_k^{\alpha_k\mu-1}}{\Gamma(\mu)\exp(\mu\rho_k^{\alpha_k})},\ \rho_k \ \geq\ 0. \tag{2.4}$$

In (2.4), $\Gamma(\cdot)$ is the Gamma function [27, id. 06.05.02.0001.01], $\alpha_k$ characterizes the non-linearity of the propagation medium at $k$-th port, and $\mu$ represents the number of multipath clusters. In a fluid antenna system, it is assumed that the port with the strongest channel condition is always selected, i.e., [5, Eq. (3)]

$$h = \max\{h_1, h_2, \cdots, h_N\}. \tag{2.5}$$

In this study, the $\alpha$-$\mu$ distribution is adopted since it is generalist, flexible, and easy to manipulate mathematically. The mentioned fading model considers a signal consisting of multipath clusters and explores the non-linearity of the propagation medium. This make the $\alpha$-$\mu$ distribution very attractive to be used in FAS. The $\alpha$-$\mu$ distribution encompasses a lot of models presented in the literature. In fact, by properly selecting the fading parameters $\alpha$ and $\mu$, the models presented in Table 2.1 can be obtained.

| Fading Models | Parameters |
|---|---|
| Rayleigh | $\alpha = 2$, $\mu = 1$ |
| Nakagami-$m$ | $\alpha = 2$, $\mu = m$ |
| Weibull | $\alpha = \alpha$, $\mu = 1$ |
| One-Gaussian | $\alpha = 2$, $\mu = 0.5$ |

**Table 2.1.** Special cases.

## 2.2 FIRST AND SECOND ORDER STATISTICS OF FAS UNDER $\alpha$-$\mu$ FADING CHANNELS

In this section, important statistics are deduced, such as PDFs, CDF, and LCR. The first order statistics are used in this work in order to derive performance metrics to evaluate the impact of the channel parameters in the FAS. Furthermore, the LCR is a key second-order statistic used to provide useful information about the dynamic temporal behavior of multipath fading channels. LCR is a statistical measure of how often a random signal crosses a certain threshold. The expressions derived are valid for any arbitrary correlation values.

### 2.2.1 Conditional PDF of $h_2$ given $h_1$

**Proposition 2.2.1.** *Let $h_2$ and $h_1 \in \mathbb{R}^+$. The conditional PDF of $h_2$ given $h_1$, denoted by $f_{h_2|h_1}(\rho_2|\rho_1)$, is written as*

$$f_{h_2|h_1}(\rho_2|\rho_1) = \frac{\mu \rho_1^{-\frac{\alpha_1}{2}(\mu-1)} \rho_2^{\frac{\alpha_2}{2}(\mu+1)-1} \alpha_2}{(1-\delta_2)\delta_2^{\frac{\mu-1}{2}}} \exp\left[-\mu\left(\frac{\rho_2^{\alpha_2}+\delta_2\rho_1^{\alpha_1}}{1-\delta_2}\right)\right] \mathrm{I}_{\mu-1}\left(\frac{2\mu\sqrt{\delta_2\rho_1^{\alpha_1}\rho_2^{\alpha_2}}}{1-\delta_2}\right), \quad (2.6)$$

*in which $\delta_2$ is the power correlation coefficient of the second port with respect to the first one and $\mathrm{I}_v(\cdot)$ is the modified Bessel function of first kind and order $v$ [27, id 03.02.02.0001.01].*

*Proof.* The PDF $f_{h_2|h_1}(\rho_2|\rho_1)$ is computed by taking a ratio of $f_{h_2,h_1}(\rho_2,\rho_1)$ over the normalized PDF of $h_1$ as

$$f_{h_2|h_1}(\rho_2|\rho_1) = \frac{f_{h_2,h_1}(\rho_1,\rho_2)}{f_{h_1}(\rho_1)}, \quad (2.7)$$

in which the joint PDF of two correlated $\alpha$-$\mu$ is given by [22, Eq. (28)]

$$f_{h_2,h_1}(\rho_1,\rho_2) = \frac{\alpha_1\alpha_2\mu^{\mu+1}\rho_1^{\frac{\alpha_1}{2}(\mu+1)-1}\rho_2^{\frac{\alpha_2}{2}(\mu+1)-1}}{(1-\delta_2)\delta_2^{\frac{\mu-1}{2}}\Gamma(\mu)} \exp\left(-\mu\frac{\rho_1^{\alpha_1}+\rho_2^{\alpha_2}}{1-\delta_2}\right)\mathrm{I}_{\mu-1}\left(\frac{2\mu\sqrt{\delta_2\rho_1^{\alpha_1}\rho_2^{\alpha_2}}}{1-\delta_2}\right). \quad (2.8)$$

Substituting (2.8) and (2.4) into $f_{h_2|h_1}(\rho_2|\rho_1)$, (2.6) can be obtained after simplifications. Hence, the proof is complete.

□

### 2.2.2 The joint PDF of $N$ correlated $\alpha$-$\mu$ random variates

**Proposition 2.2.2.** *Let $h_k \in \mathbb{R}^+$, with $k = 1, 2, \ldots, N$. The joint PDF of $N$ correlated $\alpha$-$\mu$ random variates (RV) is denoted by $f_{h_1,h_2,\ldots,h_N}(\rho_1,\rho_2,\ldots,\rho_N)$ and written as*

$$f_{h_1,h_2,\ldots,h_N}(\rho_1,\rho_2,\ldots,\rho_N) = \frac{\alpha_1 \mu^{\mu} \rho_1^{\alpha_1\mu-1}}{\Gamma(\mu)\exp\left(\mu\rho_1^{\alpha_1}\right)} \prod_{k=2}^{N} \frac{\mu\rho_1^{-\frac{\alpha_1}{2}(\mu-1)} \rho_k^{\frac{\alpha_k}{2}(\mu+1)-1} \alpha_k}{(1-\delta_k)\delta_k^{\frac{\mu-1}{2}}} \times \exp\left[-\mu\left(\frac{\rho_k^{\alpha_k}+\delta_k\rho_1^{\alpha_1}}{1-\delta_k}\right)\right] \mathrm{I}_{\mu-1}\left(\frac{2\mu\sqrt{\delta_k\rho_1^{\alpha_1}\rho_k^{\alpha_k}}}{1-\delta_k}\right). \tag{2.9}$$

*Proof.* The joint PDF of $N$ correlated $\alpha$-$\mu$ RV, $f_{h_1,h_2,\ldots,h_N}(\rho_1,\rho_2,\ldots,\rho_N)$, can be written as

$$f_{h_1,h_2,\ldots,h_N}(\rho_1,\rho_2,\ldots,\rho_N) = f_{h_1}(\rho_1) f_{h_2,\ldots,h_N|h_1}(\rho_2,\ldots,\rho_N|\rho_1). \tag{2.10}$$

Since the independence between the ports conditioned on port 1, it follows that

$$f_{h_2,\ldots,h_N|h_1}(\rho_2,\ldots,\rho_N|\rho_1) = \prod_{k=2}^{N} f_{h_k|h_1}(\rho_k|\rho_1). \tag{2.11}$$

Using (2.6), (2.11) can be written as

$$f_{h_2,\ldots,h_N|h_1}(\rho_2,\ldots,\rho_N|\rho_1) = \prod_{k=2}^{N} \frac{\mu\rho_1^{-\frac{\alpha_1}{2}(\mu-1)} \rho_k^{\frac{\alpha_k}{2}(\mu+1)-1} \alpha_k}{(1-\delta_k)\delta_k^{\frac{\mu-1}{2}}} \times \exp\left[-\mu\left(\frac{\rho_k^{\alpha_k}+\delta_k\rho_1^{\alpha_1}}{1-\delta_k}\right)\right] \mathrm{I}_{\mu-1}\left(\frac{2\mu\sqrt{\delta_k\rho_1^{\alpha_1}\rho_k^{\alpha_k}}}{1-\delta_k}\right). \tag{2.12}$$

Substituting (2.12) and (2.4) in (2.10), (2.9) is deduced, that complete the proof. □

**Corollary 2.2.2.1.** *For the case in which no correlation is considered, i.e. $\delta_k$ equals zero, it follows that*

$$f_{h_1,h_2,\ldots,h_N}(\rho_1,\rho_2,\ldots,\rho_N) = \prod_{k=1}^{N} f_{h_k}(\rho_k). \tag{2.13}$$

*Proof.* Making $\delta_k \to 0$ in (2.9), using the fact that

$$\lim_{\delta_k\to 0} \frac{\exp\left[-\mu\left(\frac{\delta_k\rho_1^{\alpha_1}+\rho_k^{\alpha_k}}{1-\delta_k}\right)\right]}{(1-\delta_k)\delta_k^{\frac{\mu-1}{2}}} \mathrm{I}_{\mu-1}\left(\frac{2\mu\sqrt{\delta_k\rho_1^{\alpha_1}\rho_k^{\alpha_k}}}{1-\delta_k}\right) = \frac{\exp\left[-\mu\rho_k^{\alpha_k}\right]}{\Gamma(\mu)} \left(\mu\sqrt{\rho_1^{\alpha_1}\rho_k^{\alpha_k}}\right)^{\mu-1} \tag{2.14}$$

and, in sequence, utilizing the result above again in (2.9), (2.13) is obtained after simplifications. Hence, the proof is complete. □

### 2.2.3 The joint CDF

**Proposition 2.2.3.** *The joint CDF of $h_1, h_2, \ldots, h_N$, denoted by $F_{h_1,h_2,\ldots,h_N}(\rho_1,\rho_2,\ldots,\rho_N)$, is given by*

$$F_{h_1,h_2,\ldots,h_N}(\rho_1,\rho_2,\ldots,\rho_N) = \frac{\alpha_1\mu^\mu}{\Gamma(\mu)}\int_0^{\rho_1} t_1^{\alpha_1\mu-1}\exp\left(-\mu t_1^{\alpha_1}\right) \times \prod_{k=2}^{N}\left[1-\mathrm{Q}_\mu\left(\sqrt{\frac{2\mu\delta_k t_1^{\alpha_1}}{1-\delta_k}},\sqrt{\frac{2\mu\rho_k^{\alpha_k}}{1-\delta_k}}\right)\right]\mathrm{d}t_1, \tag{2.15}$$

*in which $\mathrm{Q}_\mu(\cdot,\cdot)$ is the Marcum Q-function.*

*Proof.* The joint CDF of $h_1$, $h_2$, $\cdots$, $h_N$ can be evaluated by means of

$$F_{h_1,h_2,\ldots,h_N}(\rho_1,\rho_2,\ldots,\rho_N) = \int_0^{\rho_1}\cdots\int_0^{\rho_N} f_{h_1,h_2,\ldots,h_N}(t_1,t_2,\ldots,t_N)\mathrm{d}t_1\cdots\mathrm{d}t_N. \tag{2.16}$$

Replacing (2.9) in $F_{h_1,h_2,\ldots,h_N}(\rho_1,\rho_2,\ldots,\rho_N)$, using [28, Eq. (8.445)] and proceeding with some simplifications, it follows that

$$\begin{aligned} &F_{h_1,h_2,\ldots,h_N}(\rho_1,\rho_2,\ldots,\rho_N) = \\ &\quad\frac{\alpha_1\mu^\mu}{\Gamma(\mu)}\prod_{k=2}^{N}\frac{\mu^\mu\alpha_k}{(1-\delta_k)^\mu}\int_0^{\rho_1}\frac{t_1^{\alpha_1\mu-1}}{\exp(\mu t_1^{\alpha_1})}\exp\left(-\sum_{k=2}^{N}\mu t_1^{\alpha_1}\left(\frac{1}{1-\delta_k}-1\right)\right) \\ &\quad\times\left[\prod_{k=2}^{N}\sum_{i_k=0}^{\infty}\frac{1}{i_k!\Gamma(\mu+i_k)}\left(\frac{\mu^2\delta_k t_1^{\alpha_1}}{(1-\delta_k)^2}\right)^{i_k}\int_0^{\rho_k} t_k^{\alpha_k(\mu+i_k)-1}\exp\left(\frac{-\mu t_k^{\alpha_k}}{1-\delta_k}\right)\mathrm{d}t_k\right]\mathrm{d}t_1 \end{aligned} \tag{2.17}$$

can be obtained.

Applying the variable change $x = t_k^{\alpha_k}$ and using [28, Eq. (3.381.1)], the inner integral of (2.17) with respect of $t_k$ can be solved. After simplifications,

$$\begin{aligned} &F_{h_1,h_2,\ldots,h_N}(\rho_1,\rho_2,\ldots,\rho_N) = \\ &\frac{\alpha_1\mu^\mu}{\Gamma(\mu)}\int_0^{\rho_1}\frac{t_1^{\alpha_1\mu-1}}{\exp(\mu t_1^{\alpha_1})}\exp\left(-\sum_{k=2}^{N}\mu t_1^{\alpha_1}\left(\frac{1}{1-\delta_k}-1\right)\right)\left[\prod_{k=2}^{N}\sum_{i_k=0}^{\infty}\frac{(\mu\delta_k t_1^{\alpha_1})^{i_k}\gamma\left(\mu+i_k,\frac{\mu\rho_k^{\alpha_k}}{1-\delta_k}\right)}{(1-\delta_k)^{i_k}\Gamma(\mu+i_k)i_k!}\right]\mathrm{d}t_1. \end{aligned} \tag{2.18}$$

Using [28, Eq. (8.356.3)] and [29, Eq. (9)]

$$\mathrm{Q}_{\mu}(A,\beta) = \exp\left(-\frac{A^2}{2}\right)\sum_{i_k=0}^{\infty}\frac{1}{i_k!}\left(\frac{A^2}{2}\right)^{i_k}\frac{\Gamma(\mu+i_k,\beta^2/2)}{\Gamma(\mu+i_k)}, \tag{2.19}$$

then (2.15) is deduced after simplifications, with

$$A = \sqrt{\frac{2\mu\delta_k\rho_1^{\alpha_1}}{1-\delta_k}} \tag{2.20}$$

and

$$\beta = \sqrt{\frac{2\mu P_k^{\alpha_k}}{1-\delta_k}}. \tag{2.21}$$

Hence, the proof is complete. □

### 2.2.4 Level Crossing Rate

**Proposition 2.2.4.** *The LCR, denoted by $L(\rho_{\mathrm{th}})$, is the measurement of the average number of times at which the envelope $h$ crosses a certain threshold level $\rho_{\mathrm{th}}$ and, for a $N$-port FAS under $\alpha$-$\mu$ fading channels, is given by*

$$\begin{aligned} L(\rho_{\mathrm{th}}) = {} & \frac{\sqrt{2\pi}f_{\mathrm{D}}\Gamma\left(\mu-\frac{1}{2}+\frac{1}{\alpha_j}\right)}{\alpha_j\mu^{\frac{1}{\alpha_j}}\Gamma(\mu)}\frac{\mu^{\mu}\alpha_1}{\rho_{\mathrm{th}}\Gamma(\mu)} \\ & \Bigg\{\frac{\rho_{\mathrm{th}}^{\alpha_1\mu}}{\exp\left(\mu\rho_{\mathrm{th}}^{\alpha_1}\right)}\prod_{k=2}^{N}\left[1-\mathrm{Q}_{\mu}\left(\sqrt{\frac{2\mu\delta_k\rho_{\mathrm{th}}^{\alpha_1}}{1-\delta_k}},\sqrt{\frac{2\mu\rho_{\mathrm{th}}^{\alpha_k}}{1-\delta_k}}\right)\right]+\sum_{i=2}^{N}\frac{\alpha_i\mu\rho_{\mathrm{th}}^{\frac{\alpha_i}{2}(\mu+1)}}{(1-\delta_i)\delta_i^{\frac{\mu-1}{2}}\exp\left(\frac{\mu\rho_{\mathrm{th}}^{\alpha_i}}{1-\delta_i}\right)} \\ & \int_0^{\rho_{\mathrm{th}}}\frac{\rho_1^{\frac{\alpha_1}{2}(\mu+1)-1}}{\exp\left(\frac{\mu\rho_1^{\alpha_1}}{1-\delta_i}\right)}\mathrm{I}_{\mu-1}\left(\frac{2\mu\sqrt{\delta_i\rho_1^{\alpha_1}\rho_{\mathrm{th}}^{\alpha_i}}}{1-\delta_i}\right)\prod_{\substack{k=2\\k\neq i}}^{N}\left[1-\mathrm{Q}_{\mu}\left(\sqrt{\frac{2\mu\delta_k\rho_1^{\alpha_1}}{1-\delta_k}},\sqrt{\frac{2\mu\rho_{\mathrm{th}}^{\alpha_k}}{1-\delta_k}}\right)\right]\mathrm{d}\rho_1\Bigg\} \end{aligned} \tag{2.22}$$

*with $f_{\mathrm{D}}$ denoting the maximum Doppler frequency and $j = 1, 2, \cdots, N$.*

*Proof.* The LCR is mathematically given by

$$L(\rho_{\mathrm{th}}) = \int_0^{\infty}\dot{\rho}f_{\dot{h},h}(\dot{\rho},\rho_{\mathrm{th}})\mathrm{d}\dot{\rho}, \tag{2.23}$$

in which $\dot{\rho}$ is the time derivative of $\rho$ and $f_{\dot{h},h}(\cdot,\cdot)$ is the joint PDF of $h$ and $\dot{h}$. The LCR $L(\rho_{\mathrm{th}})$ can be rewritten as presented in [5, Eqs. (13) and (14)], that is composed by two terms multiplied by [5, Eq. (12)]

$$\int_0^{\infty}\dot{\rho}f_{\dot{h}_i}(\dot{\rho})\mathrm{d}\dot{\rho} = \frac{\sqrt{2\pi}f_{\mathrm{D}}\Gamma\left(\mu-\frac{1}{2}+\frac{1}{\alpha_j}\right)}{\alpha_j\mu^{\frac{1}{\alpha_j}}\Gamma(\mu)}, \forall j = 1,\cdots,N. \tag{2.24}$$

For the first term of [5, Eq. (14)], it follows that

$$\begin{aligned}
&\underbrace{\int_0^{\rho_{\text{th}}}\cdots\int_0^{\rho_{\text{th}}}}_{(N-1)-\text{fold}} f_{h_1,h_2,\ldots,h_N}(\rho_1=\rho_{\text{th}},\rho_2,\ldots,\rho_N)\underbrace{\mathrm{d}\rho_2\cdot\mathrm{d}\rho_N}_{(N-1)-\text{fold}}\\
&\overset{(a)}{=}\frac{\alpha_1\mu^{\mu}\rho_{\text{th}}^{\alpha_1\mu-1}}{\Gamma(\mu)\exp(\mu\rho_{\text{th}}^{\alpha_1})}\prod_{k=2}^{N}\int_0^{\rho_{\text{th}}}\frac{\mu\rho_{\text{th}}^{-\frac{\alpha_1}{2}(\mu-1)}\rho_k^{\frac{\alpha_k}{2}(\mu+1)-1}\alpha_k}{(1-\delta_k)\delta_k^{\frac{\mu-1}{2}}}\\
&\times\exp\left[\frac{\mu\rho_{\text{th}}^{\alpha_1}\delta_k+\mu\rho_k^{\alpha_k}}{1-\delta_k}\right]\mathrm{I}_{\mu-1}\left(\frac{2\mu\sqrt{\delta_k\rho_{\text{th}}^{\alpha_1}\rho_k^{\alpha_k}}}{1-\delta_k}\right)\mathrm{d}\rho_k\\
&\overset{(b)}{=}\frac{\alpha_1\mu^{\mu}\rho_{\text{th}}^{\alpha_1\mu-1}}{\Gamma(\mu)\exp\left(\mu\rho_{\text{th}}^{\alpha_1}\right)}\prod_{k=2}^{N}\left[1-\mathrm{Q}_{\mu}\left(\sqrt{\frac{2\mu\delta_k\rho_{\text{th}}^{\alpha_1}}{1-\delta_k}},\sqrt{\frac{2\mu\rho_{\text{th}}^{\alpha_k}}{1-\delta_k}}\right)\right],
\end{aligned}\tag{2.25}$$

where (a) is deduced using (2.10), (2.4), (2.12) and (b) follows from [28, Eq. (8.356.3)] and [29, Eq. (9)]. The second term is given by

$$\begin{aligned}
&\sum_{i=2}^{N}\underbrace{\int_0^{\rho_{\text{th}}}\cdots\int_0^{\rho_{\text{th}}}}_{(N-1)-\text{fold}} f_{h_1,h_2,\ldots,h_N}(\rho_1,\ldots,\rho_i=\rho_{\text{th}},\ldots,\rho_N)\underbrace{\mathrm{d}\rho_1\cdots\mathrm{d}\rho_N}_{(N-1)-\text{fold},\ k\neq i}\\
&=\sum_{i=2}^{N}\frac{\alpha_i\mu^{\mu+1}\rho_{\text{th}}^{\frac{\alpha_i}{2}(\mu+1)-1}}{(1-\delta_i)\delta_i^{\frac{\mu-1}{2}}\exp\left(\frac{\mu\rho_{\text{th}}^{\alpha_i}}{1-\delta_i}\right)}\\
&\times\int_0^{\rho_{\text{th}}}\frac{\alpha_1\rho_1^{\frac{\alpha_1}{2}(\mu+1)-1}}{\Gamma(\mu)\exp\left(\frac{\mu\rho_1^{\alpha_1}}{1-\delta_i}\right)}\mathrm{I}_{\mu-1}\left(\frac{2\mu\sqrt{\delta_i\rho_1^{\alpha_1}\rho_{\text{th}}^{\alpha_i}}}{1-\delta_i}\right)\prod_{\substack{k=2\\k\neq i}}^{N}\left[1-\mathrm{Q}_{\mu}\left(\sqrt{\frac{2\mu\delta_k\rho_1^{\alpha_1}}{1-\delta_k}},\sqrt{\frac{2\mu\rho_{\text{th}}^{\alpha_k}}{1-\delta_k}}\right)\right]\mathrm{d}\rho_1,
\end{aligned}\tag{2.26}$$

derived making some variables changes and using [29, Eq. (1)].

Replacing (2.24), (2.25) and (2.26) in the previous LCR expression, (2.22) is derived. □

## 2.3 PERFORMANCE ANALYSIS

### 2.3.1 Outage Probability

The OP is defined as the probability that the received signal power falls below a certain threshold. The OP for a FAS can be derived from the joint CDF given in (2.15) by making $\rho_1{=}\rho_2{=}\cdots{=}\rho_N{=}\sqrt{\Omega\gamma_{\text{th}}/\bar{\gamma}}$, n which $\gamma_{\text{th}}$ is a specified threshold, $\bar{\gamma}$ is the average SNR and

$\Omega = \mathrm{E}[h_k^2] = \Gamma\left(\mu + 2/\alpha_k\right)/(\mu^{2/\alpha}\Gamma(\mu))$ [22, Eq. (5)]. Thus,

$$P_{\text{out}} = \frac{\alpha_1 \mu^{\mu}}{\Gamma(\mu)} \int_0^{\sqrt{\frac{\Omega\gamma_{\text{th}}}{\bar{\gamma}}}} t_1^{\alpha_1\mu-1} \exp\left(-\mu t_1^{\alpha_1}\right) \prod_{k=2}^{N} \left[1 - \mathrm{Q}_{\mu}\left(\sqrt{\frac{2\mu\delta_k t_1^{\alpha_1}}{1-\delta_k}}, \sqrt{\frac{2\mu}{1-\delta_k}\left(\frac{\Omega\gamma_{\text{th}}}{\bar{\gamma}}\right)^{\frac{\alpha_k}{2}}}\right)\right] \mathrm{d}t_1. \tag{2.27}$$

An exact reduction of the OP, due to $N$-th port for an $(N-1)$-port, can be derived expanding the $N$-th factor in the product present in (2.27). The exact reduction is denoted by $\Delta P_{\text{out}}$ and is written, after simplifications, as

$$\begin{aligned}\Delta P_{\text{out}} = \frac{\alpha_1 \mu^{\mu}}{\Gamma(\mu)} \int_0^{\sqrt{\frac{\Omega\gamma_{\text{th}}}{\bar{\gamma}}}} t_1^{\alpha_1\mu-1} \exp\left(-\mu t_1^{\alpha_1}\right) \mathrm{Q}_{\mu}\left(\sqrt{\frac{2\mu\delta_N t_1^{\alpha_1}}{1-\delta_N}}, \sqrt{\frac{2\mu}{1-\delta_N}\left(\frac{\Omega\gamma_{\text{th}}}{\bar{\gamma}}\right)^{\frac{\alpha_N}{2}}}\right) \\ \times \prod_{k=2}^{N-1} \left[1 - \mathrm{Q}_{\mu}\left(\sqrt{\frac{2\mu\delta_k t_1^{\alpha_1}}{1-\delta_k}}, \sqrt{\frac{2\mu}{1-\delta_k}\left(\frac{\Omega\gamma_{\text{th}}}{\bar{\gamma}}\right)^{\frac{\alpha_k}{2}}}\right)\right] \mathrm{d}t_1.\end{aligned} \tag{2.28}$$

For the new and improved model for $\delta_k$, as defined in (2.2); considering [16, Eq. (5)] and using the same approach presented in the aforementioned article, it follows that

$$P_{\text{out}} = \int_0^{\infty} \frac{t_1^{\mu-1}}{\Gamma(\mu)} \exp\left(-t_1\right) \prod_{k=1}^{N} \left[1 - \mathrm{Q}_{\mu}\left(\sqrt{\frac{2\delta t_1}{1-\delta}}, \sqrt{\frac{2\mu}{1-\delta}\left(\frac{\Omega\gamma_{\text{th}}}{\bar{\gamma}}\right)^{\frac{\alpha_k}{2}}}\right)\right] \mathrm{d}t_1. \tag{2.29}$$

### 2.3.2 Ergodic Channel Capacity

The ergodic channel capacity $C$, for a FAS, can be derived as [2, Eq. (9)]

$$C = \int_0^{\infty} \left(\frac{1}{1+y}\right) \mathrm{Prob}\left(h > \sqrt{\frac{y}{\Theta}}\right) \mathrm{d}y. \tag{2.30}$$

Since $\mathrm{Prob}(h > a) = 1 - \mathrm{Prob}(h < a)$ and using (2.27), it follows that the ergodic channel capacity is written as

$$\begin{aligned}C = \int_0^{\infty} \left(\frac{1}{1+y}\right) \left\{1 - \frac{\alpha_1 \mu^{\mu}}{\Gamma(\mu)} \int_0^{\sqrt{\frac{\Omega y}{\bar{\gamma}}}} t_1^{\alpha_1\mu-1} \exp\left(-\mu t_1^{\alpha_1}\right)\right. \\ \left. \times \prod_{k=2}^{N} \left[1 - \mathrm{Q}_{\mu}\left(\sqrt{\frac{2\mu\delta_k t_1^{\alpha_1}}{1-\delta_k}}, \sqrt{\frac{2\mu}{1-\delta_k}\left(\frac{\Omega y}{\bar{\gamma}}\right)^{\frac{\alpha_k}{2}}}\right)\right] \mathrm{d}t_1 \right\} \mathrm{d}y.\end{aligned} \tag{2.31}$$

## 2.4 RESULTS

In this section, theoretical OP, channel capacity, and LCR curves are presented. Theoretical curves were carried out by using the MATLAB software according to the models described throughout this work.

### 2.4.1 Numerical Results

In Fig. 2.2, the OP as a function of the number of ports $N$ is presented. In this analysis, $\mu = 1.0$, $W = \{0.5,1,2\}$, $\alpha_1 = \alpha_2 = \cdots = \alpha_N = \alpha = \{0.5,2,5\}$ and $\gamma_{\text{th}}/\bar{\gamma} = -3$ dB. In Fig. 2.2, the influence of the non-linearity parameter $\alpha$ and the size $W$ in the OP is depicted. In Fig. 2.2(a), the power correlation coefficient $\delta_k$ presented in (2.1) is adopted. In Fig. 2.2(b), the OP curves are presented considering the new and improved model for $\delta_k$, as defined in (2.2).

As the number of ports or $W$ increase, the OP value in Fig. 2.2 decreases for a fixed value of $\alpha$, since the power correlation coefficient decreases. It is possible to realize in Fig. 2.2 that for a fixed value of $N$ or $W$, as $\alpha$ increases, i.e. the less severe the fading is, the lower is the value of the OP, since that $\gamma_{\text{th}} < \bar{\gamma}$. As the higher the values of $\alpha$ are, the more deterministic the channel is around the $\bar{\gamma}$ value. Therefore, when $\gamma_{\text{th}} < \bar{\gamma}$ the probability of the SNR to fall bellow of $\gamma_{\text{th}}$ decreases. As a benchmark, OP curves under Rayleigh fading are shown. In fact, by making $\mu = 1.0$, $\alpha = 2.0$ in (2.27) or (2.29), the OP expressions presented in [3, Eq. (16)] or [16, Eq. (16)] can be easily obtained, respectively. For comparison purposes, the performance of the FAS is confronted to that using the MRC technique with 2 antennas, in which it is evidenced that, for a certain number of ports, the FAS has a better performance. In Fig. 2.2(b), it is verified that the use of (2.2) allows a more realistic analysis of the FAS, in which there is a worse performance in all scenarios even for large $N$. Also in this case, FAS also outperforms a system that uses 2-antenna MRC. In both figures, the position of the values of $\Delta P_{\text{out}} = 0.013587$ and $\Delta P_{\text{out}} = 0.013596$ from (2.28) is included, that characterizes the exact reduction in OP due to 2 for 3-ports FAS under correlations given by (a) (2.1) and (b) (2.2), with $W = 2$.

Ergodic channel capacity curves as a function of $N$ are plotted in Fig. 2.3 for variable $\alpha = \{1,2,5,10\}$, fixed $\mu = 1.0$, $\bar{\gamma} = 10$ dB, and $W = 0.5$. For $\mu = 1.0$, the Weibull fading model can be obtained as a particular case of the study proposed in this work. To the best of the author knowledge, results concerning the performance of FASs under Weibull model have not been presented in the literature. Capacity curves under Rayleigh fading are also shown in Fig. 3.1 as a benchmark, in which some results of [2, Fig. 3(a)] are reproduced as special case. It should be noted that [2, Eq. (11)] can be obtained from (2.31) under $\mu = 1.0$ and $\alpha = 2.0$. From Fig. 2.3, it is noted that the capacity improves as the parameter $\alpha$ decreases.

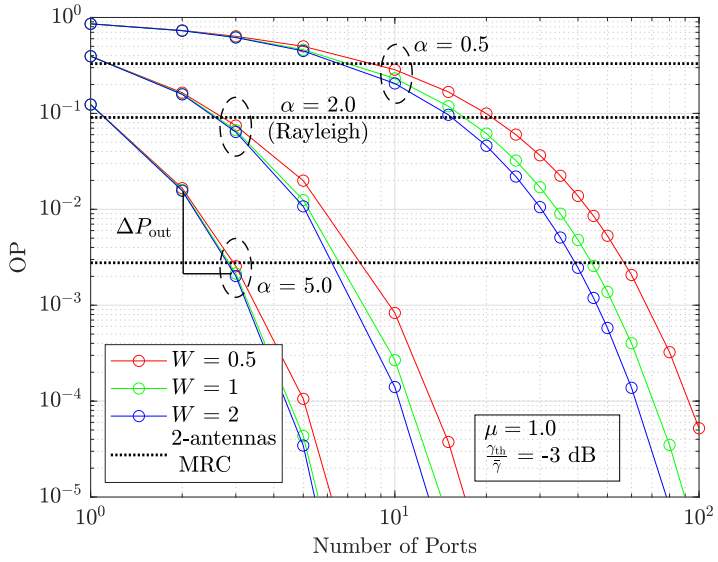


(a)

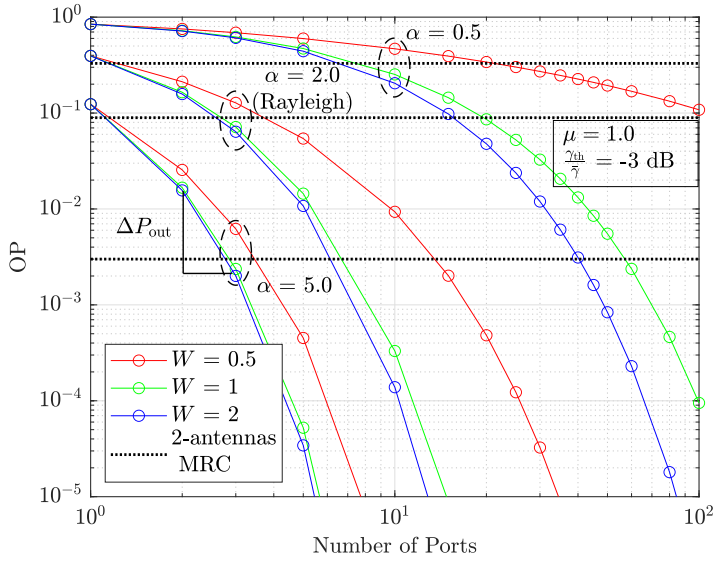


(b)

**Figure 2.2.** OP for the FAS as a function of $N$, with $\delta_k$ given by (a) (2.1) and (b) (2.2).

The normalized LCR $L(\rho_{\text{th}})/f_{\text{D}}$ as function of $N$ is shown in Fig. 2.4, with $\mu = 2.0$, $\rho_{\text{th}} =$ 25 dBm and $W = 0.2$, for different values of $\alpha = \{1{,}1.5{,}2\}$. In [4], the normalized LCR for Rayleigh channels is presented. The expression described in [4, Eq. (6)] can be also obtained from this work. As observed in Fig. 2.4, the normalized LCR decreases with the increase of the parameter $\alpha$ (i.e., the LCR improves as the channel non-linearity decreases). For comparison, the normalized LCR considering $\delta_k = 0$ are also presented, that corresponds to the case where the ports are independent. When $\delta_k = 0$, for all $\alpha$ values considered, it should be mentioned

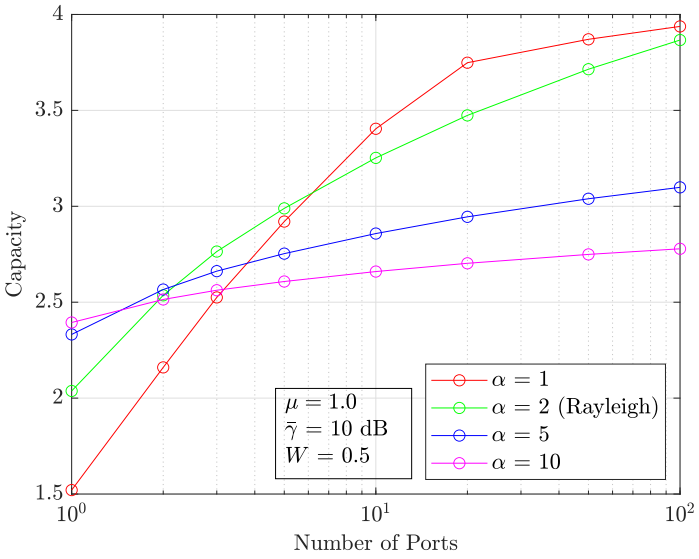


**Figure 2.3.** Ergodic channel capacity as a function of $N$.

that the LCR is better. As shown in (2.22), it should be mentioned that the normalized LCR depends of the power correlation coefficient, the decision threshold and the channel and FAS parameters.

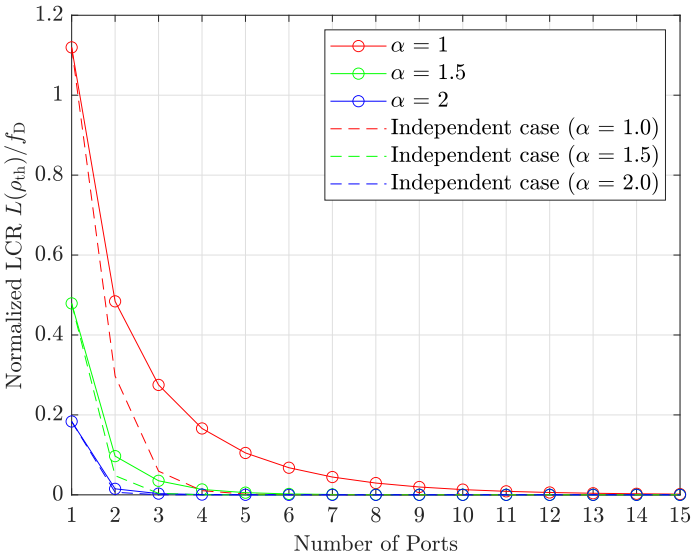


**Figure 2.4.** Normalized LCR $L(\rho_{\text{th}})/f_{\text{D}}$ as a function of $N$, under different $\alpha$ values, with $\mu = 2$, $\rho_{\text{th}} = 25$ dBm and $W = 0.2$.

CHAPTER 3

# LNN-POWERED FLUID ANTENNA MULTIPLE ACCESS

**Motivation and Outline**

In this work, for the first time, the port selection problem is framed as a MLC task under emerging and distinct FAMA scenarios, leveraging LNN alongside a more general channel fading model, the $\alpha$-$\mu$. MLC allows the ML model to focus solely on predicting the best port rather than estimating the port's CSI or SINR/SNR value, simplifying the problem [24]. Regarding the scenarios, it is considered a downlink communication system in which the base station (BS) transmits messages to users, and only one port is activated at a time [6, 7, 8]. Also, the recently proposed scenario in [17] is investigated, but in the context of FAMA, where multiple ports can be activated for a subsequent signal combination to improve receiver performance. In this case, given $N$ ports in FAMA, only the best $M$ ports are selected before performing the MRC of the branches that contain the signals received from the selected ports.

The recent fully port correlation model presented in [25] is adopted. Furthermore, a hyperparameter optimization framework is employed to find optimal LNN-based architectures for each number of observed ports. The results are compared with those in the literature, demonstrating better capabilities in predicting the best port and thus achieving lowered OP values. It is considered LNNs due to their superior capabilities in real-time modeling and adaptation to dynamic channel changes and their ability to efficiently capture temporal and spatial dependencies that allow predicting the port that maximizes SINR [26]. This approach offers an effective and scalable alternative to traditional techniques. It mitigates the challenges of obtaining signal quality metrics or CSI for all ports and improves the feasibility and performance of FAMA systems. The $\alpha$-$\mu$ fading model is adopted as the channel between the BS and the users since the aforementioned fading model is supported by experimental results and characterized by physical parameters [22].

## 3.1 SYSTEM MODEL

### 3.1.1 FAMA

A downlink communication system model is considered, where a BS transmits messages to $U$ users [6, 7]. The BS is equipped with $U$ antennas, each dedicated to transmitting signals to a specific user in the downlink. On the user side, each device is equipped with an $N$-port FAS. The system adopts a feasible and practical implementation of FAMA, commonly referred to in the literature as s-FAMA [8].

In this approach, the selected antenna port remains fixed until the channel conditions change. Notably, as highlighted in [6], FAMA simplifies multiple access by reducing it to a port selection task on the user side, eliminating the need for pre-coding or CSI at the BS. A conceptual architecture for FAMA is illustrated in Fig. 3.1, which depicts a network consisting of a BS and user equipment equipped with a fluid antenna.

In this system, the fluid antenna is an electronically reconfigurable structure technology. It comprises a linear array of predefined positions, referred to as ports, where the radiating element is dynamically switched to optimize a reception metric. In Fig. 3.1, $W$ represents the normalized size of the fluid antenna, while $\lambda$ denotes the propagation wavelength.

The signal received at the $k$-th port of the $u$-th user equipped with a fluid antenna is given by [8, Eq. (1)]

$$y_k^{(u)} = s_u g_k^{(u,u)} + \sum_{\substack{\tilde{u}=1 \\ \tilde{u}\neq u}}^{U} s_{\tilde{u}} g_k^{(\tilde{u},u)} + \eta_k^{(u)}, \tag{3.1}$$

where $s_u$ denotes the symbol transmitted to the $u$-th user with power $\sigma_{\mathrm{s}}^2$, $g_k^{(u,u)}$ denotes the channel gain between the $u$-th BS antenna and the $k$-th port of the $u$-th user, $g_k^{(\tilde{u},u)}$ denotes the channel gain between the $\tilde{u}$-th BS antenna and the $k$-th port of the $u$-th user, acting as interference on this port, and $\eta_k^{(u)}$ represents the AWGN with variance $\sigma_\eta$. The channel gains are assumed to follow the $\alpha$-$\mu$ distribution and the correlation model presented in [25] is adopted.

In FAMA, the objective is to maximize the instantaneous SINR across all $N$ ports of the

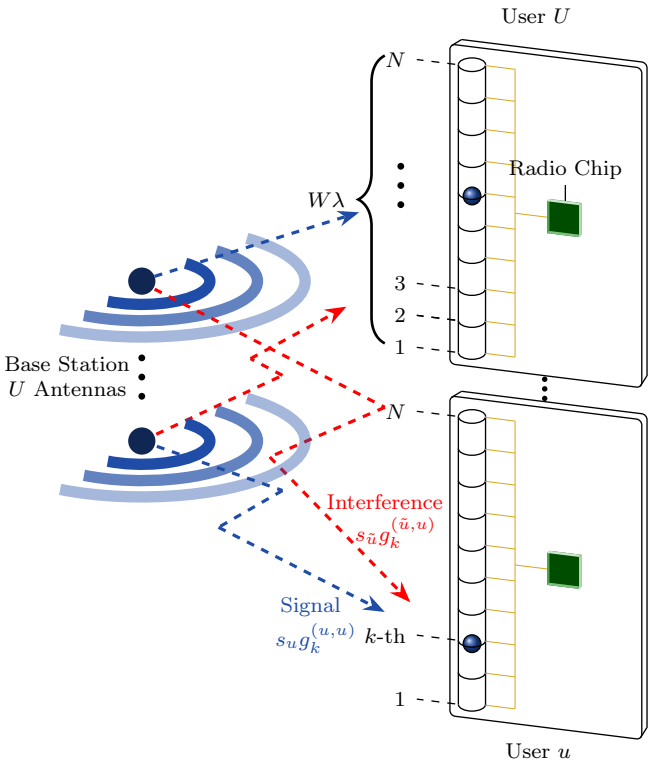


**Figure 3.1.** A possible architecture for FAMA.

$u$-th user, which is given by [19, Eq. (7)]

$$\gamma_k^{(u)} = \frac{\sigma_s^2 |g_k^{(u,u)}|^2}{\sigma_s^2 \sum_{\substack{\tilde{u}=1 \\ \tilde{u}\neq u}}^{U} |g_k^{(\tilde{u},u)}|^2 + \sigma_\eta^2}. \tag{3.2}$$

In the scenario previously described, it should be noted that only one port is activated at a time. However, it is also analyzed the recent approach proposed in [17], where multiple ports can be activated for a subsequent signal combination to improve the receiver performance. In this scenario, only the best $M$ out of $N$ available ports are selected and combined using MRC. In [17], the port selection problem has not been investigated in FAS or FAMA contexts. Therefore, this is another original contribution of this work.

### 3.1.2 Correlation Model

In FAMA, the correlation effect occurs because the ports are close to each other. The channel correlation coefficient between any two ports follows the Jakes model, written as [25]

$$\mathbb{E}[g_k g_l^\star] = \phi_{k,l} = J_0\left(\frac{2\pi(k-l)W}{N-1}\right) \tag{3.3}$$

where $\mathbb{E}[\cdot]$ denotes the expectation operator. Defining $\mathbf{\Phi} \triangleq [\phi_{k,l}]$ and with (3.3), require that

$$\mathbf{\Phi} = \mathbb{E}[\mathbf{g}\mathbf{g}^{\dagger}] = \mathbf{A}\mathbf{A}^{\dagger}, \tag{3.4}$$

where $\mathbf{g} \triangleq [g_1 \cdots g_N]$. Using eigenvalue decomposition, write $\mathbf{\Phi} = \mathbf{V}\mathbf{D}\mathbf{V}^{\dagger}$ where $\mathbf{D}$ is a diagonal matrix containing the eigenvalues and $\mathbf{V}$ is a unitary matrix of eigenvectors. As a result, $\mathbf{A}$ can be chosen as $\mathbf{A} = \mathbf{V}\mathbf{D}^{\frac{1}{2}}$ to satisfy (3.3).

### 3.1.3 Port Selection

In FAS or FAMA systems, the port with the highest SNR or SINR is always assumed to be selected. This search process is straightforward if the receiver knows all the channel gains. However, the number of ports in FAS or FAMA is considerable. Therefore, estimating the channel gain for all ports can be impractical from a computational and cost perspective.

In the scenario where only a small subset of ports, $\mathcal{M}$, is observed, the port selection problem becomes [11]

$$\mathcal{K} = \arg \underset{k \in \mathcal{N}}{K} \max\{\{\gamma_k^{(u)}\}_{k \in \mathcal{M}}, \{\tilde{\gamma}_k^{(u)}\}_{k \in \mathcal{Z}}\}, \tag{3.5}$$

in which $\mathcal{K}$ is the set of indices of the optimal ports, $K$ indicates the number of indices of ports with the highest values (i.e., highest SINR) to select out of the set of all available ports, $\mathcal{N}$, $\mathcal{M}$ represents the set of indices of port values (i.e., SINR) known by direct observation, $\mathcal{Z}$ represents the set of indices of port values obtained by other means (e.g., ML models), and $\tilde{\gamma}_k^{(u)}$ represents the port value acquired for the $k$-th non-observed port. Note that $\mathcal{N} = \mathcal{M} \cup \mathcal{Z}$ and that $K > 1$ is used for implementing MRC.

This work introduces a novel approach to the port selection problem by treating it as a classification task, bypassing the need to predict the actual SINR value, i.e., a regression task. Instead, the port selection problem is framed as an MLC task, where the model predicts the indices of the $M$ ports (i.e., classes) more likely to have the highest SINR values. Once the model predicts indices, not the actual SINR values, the FAS must observe the ports corresponding to the $K$ optimal indices.

### 3.1.4 Performance Evaluation Metric

The performance evaluation of FAMA is conducted using the OP metric, denoted as $P_{\text{out}}$. Note that $P_{\text{out}}$ represents the probability that the SINR falls below a threshold $\gamma_{\text{th}}$. In FAMA, $P_{\text{out}}$ for a user $u$ employing the MRC technique can be calculated using (3.2) as

$$P_{\text{out}} = \text{Prob}\left(\gamma_{\text{MRC}}^{(u)} < \gamma_{\text{th}}\right), \tag{3.6}$$

where

$$\gamma_{\text{MRC}}^{(u)} = \frac{\sigma_{\text{s}}^2 \sum_{n\in\mathcal{K}} |g_n^{(u,u)}|^2}{\sigma_{\text{s}}^2 \sum_{n\in\mathcal{K}} \sum_{\substack{\tilde{u}=1 \\ \tilde{u}\neq u}}^{U} |g_n^{(\tilde{u},u)}|^2 + K\sigma_\eta^2}. \tag{3.7}$$

## 3.2 DEEP LEARNING-BASED PORT SELECTION

### 3.2.1 LSTM

LSTM is a recurrent neural network architecture widely applied across various practical contexts. Due to its memory retention characteristics, it is commonly used to model time series data. However, it has been employed to model spatially correlated signals at the antenna ports in FAS and FAMA. In [11, 19], LSTM performs a regression task predicting channel conditions based on a subset of observed ports. It enables port selection by estimating the gains of unobserved ports through its predictive capability. Using supervised learning and analyzing the port selection problem as a regression task, the LSTM model is trained to predict the SINR values of the $N$ ports, considering the mean squared error (MSE) as the loss function.

### 3.2.2 LNN

LNNs are first introduced in [30] to enhance the stability of dynamic time series through a specialized layer known as the liquid layer, which incorporates solvers for ordinary differential equations (ODEs). Unlike traditional recurrent neural networks, such as LSTM, LNNs feature an adaptive structure that modifies dynamically in response to new data, enabling more efficient processing and improved energy utilization. This adaptability allows LNNs to be trained faster and with fewer computational resources than conventional recurrent neural networks, such as

LSTM networks.

At the core of LNNs is the liquid time constant (LTC) layer, which relies on ODEs to adjust dynamically to input data changes over time [30, 31]. Although these equations increase computational complexity, they allow the network to adapt to evolving data patterns. LTCs have been applied in various fields, including time series forecasting for training autonomous vehicles, channel estimation, and vehicle traffic modeling. In this work, LNNs are employed to predict spatially correlated channels.

### 3.2.3 Optuna-aided Optimization

This work employs a hyperparameter optimization framework, Optuna, to identify optimal liquid-layer-based neural network architectures tailored to different numbers of observed ports [32]. This framework conducts multiple training sessions across various neural network architectures. The following hyperparameters are adjusted to minimize the defined classification error for different numbers of observed ports: application of preprocessing techniques, such as principal component analysis (PCA) and scaling; number and types of layers, including liquid (LNN), convolutional (CNN) and dense (DNN) layers; number of filters, cells, and units in the convolutional, liquid, and dense layers, respectively; choice of optimizers; loss functions; and learning rate. Consequently, optimized architectures are determined for each configuration of observed ports.

As mentioned, the port selection problem is framed as an MLC task, where the LNN-based models are trained to predict the set of $M$ port indices with the highest probability values. $M$ is a hyperparameter that must be optimized as well. The models' performance is assessed using F1-score or binary cross-entropy as the loss function.

## 3.3 RESULTS

### 3.3.1 Parameter Configuration

The data considered in this study are generated using MATLAB software, assuming that the $\alpha$-$\mu$ probability distribution characterizes the channel's envelope gains using (3.2). The neural network models based on LSTM and LNN layers are implemented in Python using the TensorFlow framework [33]. The generated data are divided into two parts: the input attributes, which are the values of the subset of observed ports, and labels, which are the output values of the models. In the case of LSTM-based models, the labels correspond to the raw data generated, i.e., the actual SINR values read across all $N$ ports, since the port selection problem is addressed as a regression task. For the LNN-based models, where MLC is assumed, the labels corresponding to the $M$ highest values among the $N$ ports are represented by values equal to 1, meaning their probability of presenting one of the $M$ highest SINR values is one. In contrast, the other labels (i.e., $N - M$) are represented by values equal to 0, meaning their probability of presenting one of the $M$ highest SINR values is zero. The dataset for both cases is divided into training, validation, and testing sets, with percentages of 70%, 15%, and 15%, respectively, with 500.000 samples for each training parameter configuration. It is assumed that the samples in the validation and testing sets are unseen by the trained model, meaning the model is not presented with them during training.

This study considers a linear structure of the fluid antenna and that the average SNR at each UE is set to 40 dB. Furthermore, the observed ports are chosen to be uniformly distributed over $W\lambda$ to explore more effectively the correlation effect. It should be mentioned the results obtained with the LSTM-based architecture presented in [19] are used for comparison with the results. Additionally, the optimal hyperparameters for the LNN-based architectures for each observed port count are in Table 3.1, optimized by Optuna with 50 trials and 50 epochs of training for the Rayleigh case (when $\alpha = 2$ and $\mu = 1$). This are available in a public repository, along with the source code needed to reproduce the findings [1]. In the mentioned repository, we also provide a discussion of the computational complexity of the model and its convergence, as well as the computational cost under different settings.

[1]The code is available at: https://github.com/AlvimPedro/LNN-FAMA

| *Parameters* | *5 Ports* | *6 Ports* | *7 Ports* | *8 Ports* | *9 Ports* | *10 Ports* |
|---|---|---|---|---|---|---|
| CNN Layers | 0 | 0 | 0 | 0 | 0 | 0 |
| CNN Filters | - | - | - | - | - | - |
| CNN Kernel Size | - | - | - | - | - | - |
| Pooling Layer | - | - | - | - | - | - |
| LNN Layers | 1 | 1 | 2 | 1 | 1 | 1 |
| LNN Cells (1º Layer) | 28 | 15 | 69 | 34 | 64 | 94 |
| LNN Cells (2º Layer) | - | - | 77 | - | - | - |
| LNN Cells (3º Layer) | - | - | - | - | - | - |
| Dense Layers | 2 | 2 | 2 | 2 | 1 | 2 |
| Dense Cells (1º Layer) | 180 | 277 | 268 | 269 | 188 | 125 |
| Dropout (1º Layer) | 30% | 0% | 30% | 20% | 40% | 10% |
| Dense Cells (2º Layer) | 106 | 99 | 272 | 176 | - | 256 |
| Dropout (2º Layer) | 40% | 50% | 40% | 30% | - | 40% |
| Dense Cells (3º Layer) | - | - | - | - | - | - |
| Dropout (2º Layer) | - | - | - | - | - | - |
| Optimizer | Adam | Nadam | Nadam | Adam | Adam | Nadam |
| Scaler | None | MinMax | MinMax | None | Standard | MinMax |
| PCA | No | Yes | No | No | No | No |
| Loss Function | Binary Cross Entropy | Binary Cross Entropy | Binary Cross Entropy | Binary Cross Entropy | Binary Cross Entropy | Binary Cross Entropy |
| Learning Rate | 0.000277 | 0.000132 | 0.000071 | 0.000069 | 0.000078 | 0.000053 |
| Last Dense Layer with Sigmoid Activation | 100 | 100 | 100 | 100 | 100 | 100 |

**Table 3.1.** Hyperparameter optimization by Optuna.

### 3.3.2 Selecting the Number of Classes, $M$

Table 3.2 compares the OP attained when Optuna is employed to find optimized LNN-based architectures for each number of classes, $M$, and observed ports with the parameters listed in the bottom-left box of Fig. 3.2. Then, using each optimized architecture, the port selected for

| | Number of classes, $M$ | | | |
|---|---|---|---|---|
| **Number of observed ports** | **1** | **3** | **5** | **10** |
| 5 | 0.1904 | 0.1881 | 0.1890 | 0.1901 |
| 6 | 0.1543 | 0.1494 | 0.1507 | 0.1502 |
| 7 | 0.1107 | 0.1089 | 0.1091 | 0.1089 |
| 8 | 0.0839 | 0.0834 | 0.0842 | 0.0863 |
| 9 | 0.0703 | 0.0686 | 0.0690 | 0.0709 |
| 10 | 0.0561 | 0.0544 | 0.0554 | 0.0549 |
| 11 | 0.0457 | 0.0446 | 0.0474 | 0.0448 |
| 13 | 0.0287 | 0.0281 | 0.0281 | 0.0293 |
| 15 | 0.0212 | 0.0211 | 0.0218 | 0.0223 |

**Table 3.2.** OP for different number of classes, $M$, versus the number of observed ports.

calculating the OP is the one meeting (3.5) when $K = 1$. The table shows that $M = 3$ is the best number of classes since it produces the lowest OP across all considered numbers of observed ports. Therefore, it is make $M = 3$ henceforward for all subsequent results.

### 3.3.3 Performance Analysis

As a function of the number of observed ports, OP curves are presented in Fig. 3.2 for s-FAMA, considering the proposed optimized LNN-based architectures and the LSTM-based one presented in [19]. The ideal-case curve corresponds to the situation where the gain of all ports is available for the subsequent selection of the best one. Note that this curve can be interpreted as an upper bound. The reference-case curve refers to the case where the one-best port is selected only among the set of observed ones, meaning that the highest value among the observed ports is chosen. The OP decreases as the number of observed ports increases.

The optimized LNN-based models perform better than the LSTM-based model presented in the literature [19]. For 20% of the observed ports, the LNN performance is already close to the ideal case, tending to it as the number of ports increases. The dark-blue and red curves used the methodology adopted in [19], which selects the port with the highest SINR among those observed and the one indicated by the model (*i.e.*, the port with the index predicted by the model as having the highest SINR), as expressed by (3.5).

Additionally, that methodology is extended to include a subset of ports indicated by the model as having the highest probabilities in the port selection problem. This modified method-

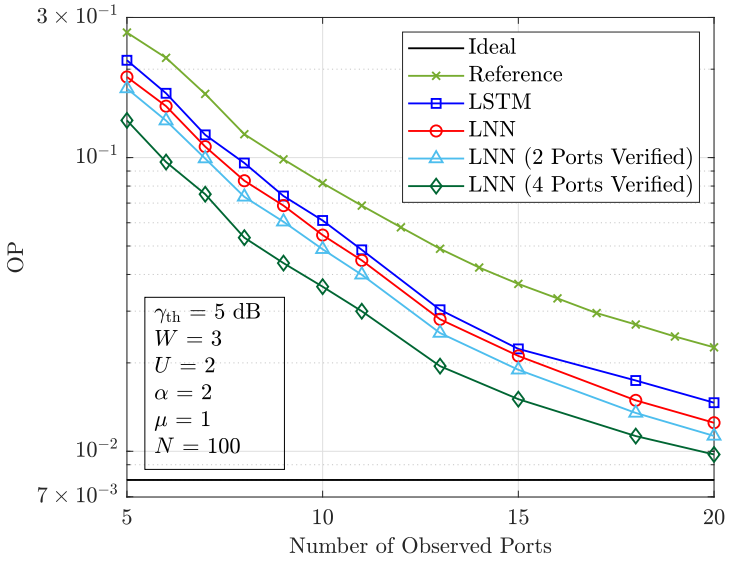


**Figure 3.2.** OP curves as a function of the number of observed ports for s-FAMA.

ology selects the port with the highest SINR among those observed and the subset of ports indicated by the model. The results of this selection methodology are illustrated in Fig. 3.2 by the light-blue and dark-green curves, where the SINR values of a subset of 2 and 4 ports indicated by the model are also considered for the port selection, respectively. As can be seen, this approach improves the OP performance, but to the detriment of a higher computational complexity.

Fig. 3.3 presents OP curves as a function of the number of observed ports for different numbers of combined ports. It is considered the scenario in which multiple ports can be activated for subsequent signal combinations to enhance the receiver's performance. In this case, $K$ is set to a value greater than 1, i.e., 2, 4, and 6 ports, respectively. In this case, s-FAMA and the MRC technique are combined. As expected, for a given number of observed ports, the OP decreases as the number of combined ports increases. As the number of combined ports increases, the gap between the reference curve and the one predicted by the LNN model gets wider. This is a direct consequence of combining more ports since the probability of getting a port with SINR above the threshold is higher. Notably, from 15 observed ports onward, the proposed LNN-based model's predictions align with the ideal-case curve across all scenarios considering 2, 4, and 6 combined ports. However, it should be noted that the increased system robustness concerning OP has the disadvantage of increased complexity and cost, as more radio frequency chains and higher processing of received signals are required.

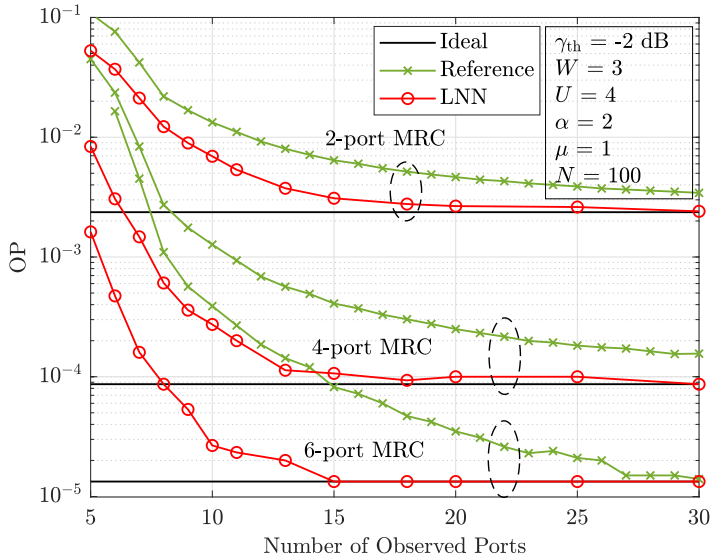


**Figure 3.3.** OP curves as a function of the number of observed ports, under s-FAMA, with different values for the MRC branches.

Figs. 3.4(a) and (b) highlight the impact of channel non-linearity and fading intensity on the OP, respectively. For $\mu = 1$, the Weibull fading model can be obtained as a particular case of the study proposed in this work. To the best of the author knowledge, the literature does not present results for the port selection under FAMA considering the Weibull model. The following insights are perceived where the OP improves: (i) as the number of observed ports increases; (ii) as $\alpha$ and/or $\mu$ decreases. In fact, to provide multiple access, the FAMA system utilizes the deep fades of interference, which occur more frequently in harsh environments (i.e., the FAMA system has more opportunities to exploit signal envelope variations and peaks). Note that the LNN can predict the optimal port even for different values of $\alpha$ and $\mu$, yielding near-ideal results comparable to those in other scenarios for 20 observed ports. This shows the capability of the LNN to perform effectively across various conditions.

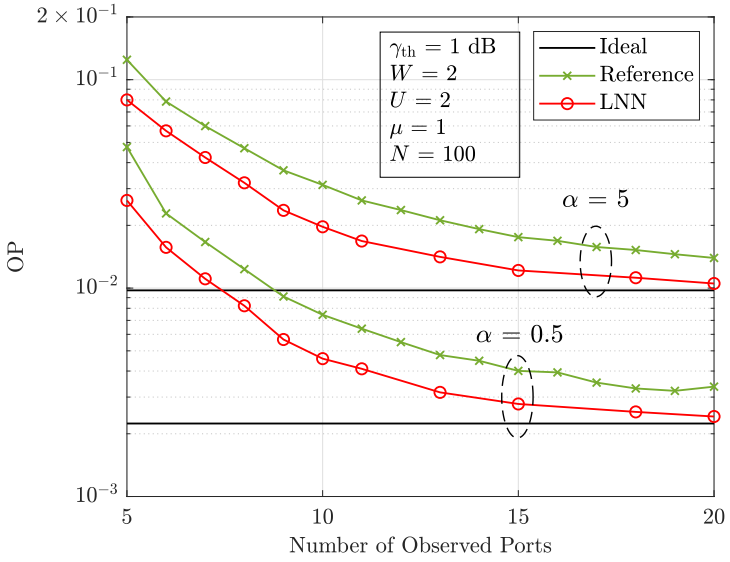


(a)

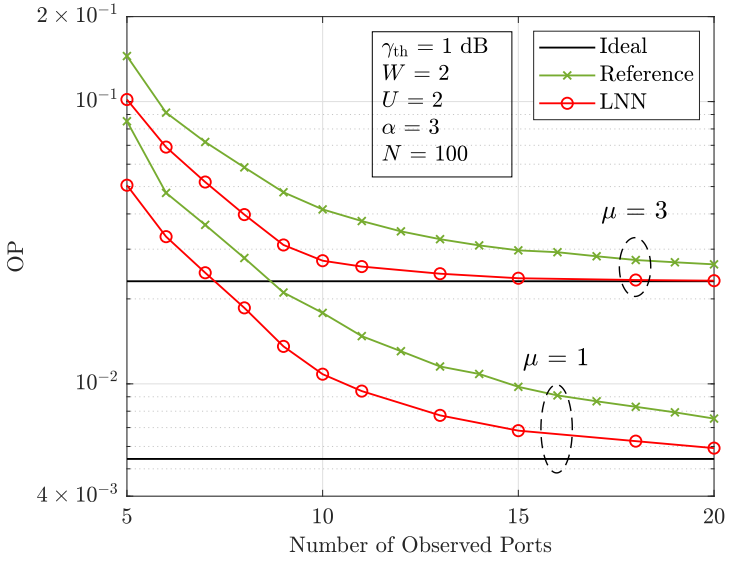


(b)

**Figure 3.4.** OP curves as a function of the number of observed ports, under s-FAMA, for different values of (a) $\alpha$ and (b) $\mu$.

CHAPTER 4

# CONCLUSIONS

This thesis has advanced the knowledge of FAS under $\alpha$-$\mu$ fading channels. In the mentioned context, important statistics were derived, such as the PDFs, CDF, and LCR. Metrics such as the OP and ergodic channel capacity were also deduced. Furthermore, an exact reduction of the OP due to $N$-th port for an $(N-1)$-port were also presented. Curves were shown for the OP and ergodic channel capacity as a function of the number of the ports under different parameters of fading model and the system, in which some insights were perceived. Furthermore, some results available in the literature were reproduced as particular cases of the study proposed. Also, has advanced knowledge concerning the port selection problem under FAMA scenarios over $\alpha$-$\mu$ fading channels. A new approach employing LNN-based models as multi-label classifiers has been presented to predict the port indices that maximize the SINR. Furthermore, an optimization framework was demonstrated to find optimal LNN-based architectures under different numbers of observed ports. Unprecedented scenarios were analyzed, including the combination of port selection with MRC. This new approach improved the system performance in terms of OP.

As future works:

- FAS has emerged as a hot topic in recent years, demonstrating promising results. Furthermore, it can be seamlessly integrated with other advanced communication technologies, including MIMO, non-orthogonal multiple access (NOMA), unmanned aerial vehicle (UAV), and RIS. However, these integrations still need to be comprehensively analyzed under more realistic fading conditions. Furthermore, the port selection problem has been thoroughly investigated in such scenarios.

- Evaluate the theoretical statistics of FAMA scenario under $\alpha$-$\mu$ fading channels.

- The analytical modeling of FAS and FAMA has not yet been extended to more com-

plex and realistic fading models, such as the $\alpha$-$\mathcal{F}$ distribution, which considers pointing errors. However, the mathematical complexities involved in such formulations increase significantly, representing a substantial challenge.

# BIBLIOGRAPHY


[1] K. -K. Wong and K. -F. Tong, Y. Zhang and Z. Zhongbin, "Fluid Antenna System for 6G: When Bruce Lee Inspires Wireless Communications," *Electron. Lett.*, vol. 56, no. 24, pp. 1288-1290, Nov. 2020. Cited on page 1.

[2] K. K. Wong, A. Shojaeifard, K. -F. Tong and Y. Zhang, "Performance Limits of Fluid Antenna Systems," *IEEE Commun. Lett.*, vol. 24, no. 11, pp. 2469-2472, Nov. 2020. Cited 5 times on pages 1, 6, 7, 14, and 15.

[3] K. -K. Wong, A. Shojaeifard, K. -F. Tong and Y. Zhang, "Fluid Antenna Systems," *IEEE Trans. Wirel. Commun.*, vol. 20, no. 3, pp. 1950-1962, Mar. 2021. Cited 5 times on pages 1, 6, 7, 8, and 15.

[4] L. Tlebaldiyeva, G. Nauryzbayev, S. Arzykulov, A. Eltawil and T. Tsiftsis, "Enhancing QoS Through Fluid Antenna Systems over Correlated Nakagami-$m$ Fading Channels," in *Proc. of the IEEE WCNC*, pp. 78-83, 2022. Cited 3 times on pages 1, 6, and 16.

[5] P. Mukherjee, C. Psomas and I. Krikidis, "On the Level Crossing Rate of Fluid Antenna Systems," in Proc. of the *IEEE SPAWC*, pp. 1-5, 2022. Cited 4 times on pages 1, 8, 12, and 13.

[6] K. -K. Wong and K. -F. Tong, "Fluid Antenna Multiple Access," *IEEE Trans. Wirel. Commun.*, vol. 21, no. 7, pp. 4801-4815, Jul. 2022. Cited 4 times on pages 1, 2, 18, and 19.

[7] K. -K. Wong, K. -F. Tong, Y. Chen and Y. Zhang, "Fast Fluid Antenna Multiple Access Enabling Massive Connectivity," *IEEE Commun. Lett.*, vol. 27, no. 2, pp. 711-715, Fev. 2023. Cited 4 times on pages 1, 2, 18, and 19.

[8] K. -K. Wong et al., "Slow Fluid Antenna Multiple Access," *IEEE Trans. Commun.*, vol. 71, no. 5, pp. 2831-2846, May 2023. Cited 4 times on pages 1, 2, 18, and 19.

[9] C. Skouroumounis and I. Krikidis, "Large-Scale Fluid Antenna Systems With Linear MMSE Channel Estimation," in Proc. of the *IEEE ICC*, pp. 1330-1335, 2022. Cited 2 times on pages 1 and 2.

[10] A. Shojaeifard et al., "MIMO Evolution Beyond 5G Through Reconfigurable Intelligent Surfaces and Fluid Antenna Systems," in Proc. of the *IEEE*, vol. 110, no. 9, pp. 1244-1265, Sep. 2022. Cited 2 times on pages 1 and 2.

[11] Z. Chai, K. -K. Wong, K. -F. Tong, Y. Chen and Y. Zhang, "Port Selection for Fluid Antenna Systems," *IEEE Commun. Lett.*, vol. 26, no. 5, pp. 1180-1184, May 2022. Cited 5 times on pages 1, 2, 3, 21, and 22.

[12] Z. Chai, K. -K. Wong, K. -F. Tong, Y. Chen and Y. Zhang, "Performance of Machine Learning Aided Fluid Antenna System with Improved Spatial Correlation Model," in Proc. of the *IEEE 6GNet*, pp. 1-6, 2022. Cited 3 times on pages 1, 2, and 3.

[13] K. -K. Wong et al., "Fluid Antenna System—Part I: Preliminaries," *IEEE Commun. Lett.*, vol. 27, no. 8, pp. 1919-1923, Aug. 2023. Cited on page 1.

[14] K. -K. Wong, K. -F. Tong and C. -B. Chae, "Fluid Antenna System—Part II: Research Opportunities," *IEEE Commun. Lett.*, vol. 27, no. 8, pp. 1924-1928, Aug. 2023. Cited on page 1.

[15] K. -K. Wong, K. -F. Tong and C. -B. Chae, "Fluid Antenna System—Part III: A New Paradigm of Distributed Artificial Scattering Surfaces for Massive Connectivity," *IEEE Commun. Lett.*, vol. 27, no. 8, pp. 1929-1933, Aug. 2023. Cited on page 1.

[16] K. K. Wong, K. F. Tong, Y. Chen, and Y. Zhang, "Closed-Form Expressions for Spatial Correlation Parameters for Performance Analysis of Fluid Antenna Systems," *Electron. Lett.*, vol. 58, no. 11, pp. 453-457, May 2022. Cited 6 times on pages 2, 3, 7, 8, 14, and 15.

[17] X. Lai et al., "On Performance of Fluid Antenna System using Maximum Ratio Combining", *IEEE Commun. Lett.*, vol. 28, no. 2, pp. 402-406, Fev. 2024. Cited 3 times on pages 2, 18, and 20.

[18] A. F. M. S. Shah etal., "A Survey on Fluid Antenna Multiple Access for 6G: A New Multiple Access Technology That Provides Great Diversity in a Small Space," *IEEE Access*, vol. 12, pp. 88410-88425, Jun. 2024. Cited on page 2.

[19] N. Waqar et al., "Deep Learning Enabled Slow Fluid Antenna Multiple Access," *IEEE Commun. Lett.*, vol. 27, no. 3, pp. 861-865, Mar. 2023. Cited 6 times on pages 2, 3, 20, 22, 24, and 26.

[20] S. Zhang et al., "Fast Port Selection using Temporal and Spatial Correlation for Fluid Antenna Systems," in Proc. of *IEEE Statistical Signal Processing Workshop*, pp. 95-99, 2023. Cited 2 times on pages 2 and 3.

[21] M. Eskandari et al., "cGAN-Based Slow Fluid Antenna Multiple Access," *IEEE Wirel. Commun. Lett.*, vol. 13, no. 10, pp. 2907-2911, Oct. 2024. Cited 2 times on pages 2 and 3.

[22] M. D. Yacoub, "The $\alpha$-$\mu$ Distribution: A Physical Fading Model for the Stacy Distribution," *IEEE Trans. Veh. Technol.*, vol. 56, no. 1, pp. 27-34, Jan. 2007. Cited 5 times on pages 6, 8, 9, 14, and 18.

[23] E. N. Papasotiriou et al., "An Experimentally Validated Fading Model for THz Wireless Systems," Sci. Rep., vol. 11, no. 18717, pp. 1-14, Set. 2021. Cited on page 6.

[24] Z.-H. Zhou. "Machine Learning." Springer nature, 2021. Cited on page 18.

[25] M. Khammassi, A. Kammoun and M. -S. Alouini, "A New Analytical Approximation of the Fluid Antenna System Channel," *IEEE Trans. Wirel. Commun.*, vol. 22, no. 12, pp. 8843-8858, Dec. 2023. Cited 3 times on pages 18, 19, and 20.

[26] F. Zhu et al, "Robust Continuous-Time Beam Tracking with Liquid Neural Network, *ArXiv*, pp. 1-6, Aug. 2024. Cited on page 18.

[27] Wolfram Research, Inc. (2020). *Wolfram Research*. Accessed: Dec. 16, 2022. [Online]. Available: http://functions.wolfram.com/id. Cited 2 times on pages 8 and 9.

[28] I. S. Gradshteyn and I. M. Ryzhik. *Table of Integrals, Series and Products*. New York: Academic Express, 2007. Cited 3 times on pages 11, 12, and 13.

[29] A. Annamalai, C. Tellambura and J. Matyjas, "A New Twist on the Generalized Marcum Q-Function $Q_M(a, b)$ with Fractional-Order $M$ and Its Applications," in Proc. of the *IEEE CCNC*, pp. 1-5, 2009. Cited 2 times on pages 12 and 13.

[30] R. Hasani et al., "Liquid Time-Constant Networks", in Proc. of *AAAI Conference on Artificial Intelligence*, vol. 35, no. 9, 2021. Cited 2 times on pages 22 and 23.

[31] R. Hasani et al., "Closed-Form Continuous-Time Neural Networks," *Nature Machine Intelligence*, vol. 4, no. 11, pp. 992-1003, Nov. 2022. Cited on page 23.

[32] T. Akiba et al., "Optuna: A Next-Generation Hyperparameter Optimization Framework", in Proc. of *25th ACM SIGKDD International Conference on Knowledge Discovery & Data Mining*, 2019. Cited on page 23.

[33] P. Singh et al., "Introduction to Tensorflow 2.0 - Learn TensorFlow 2.0: Implement Machine Learning and Deep Learning Models with Python", pp. 1-24, 2020. Cited on page 24.